Spin dynamics of wave packets evolving with the Dirac Hamiltonian in atoms with high atomic number Z

R. Arvieu, P. Rozmej, M. Turek

Spin dynamics of wave packets evolving with the Dirac Hamiltonian in atoms with high Z

R Arvieu† P Rozmej‡ and M Turek‡‖

‡Institut des Sciences Nucléaires, F-38026 Grenoble, France
†Instytut Fizyki, Uniwersytet MCS, 20-031 Lublin, Poland

Abstract. The motion of circular WP for one electron in central Coulomb field with high Z is calculated. The WP is defined in terms of solutions of the Dirac equation in order to take into account all possible relevant effects in particular the spin-orbit potential. A time scale is defined within which spin dynamics must be taken into account mainly in the atoms with high Z. Within this time scale there exists a mechanism of collapses and revivals of the spin already shown by the authors for harmonic oscillator potential and called the *spin orbit pendulum*. However this effect has not the exact periodicity of the simpler model, but the WP's spatial motion is nevertheless quite similar.

PACS numbers: 03.65.Sq

Submitted to *Physical Review A* 22 February 2000

1. Introduction

In the last decade large efforts [1–7] have been devoted to the detailed understanding of the quantum dynamics of WP in simple systems like H atoms or hydrogenoid atoms. Theoretical investigations resulted in very good understanding of such subtle interference effects like collapse, revivals, fractional revivals and super-revivals of wavepackets created in atomic and molecular systems. Many signatures of these phenomena have been observed in numerous sophisticated experimental studies. Indeed with contemporary lasers and tunable electromagnetic fields one can engineer many different desired initial states and analyze their time evolution [8].

Our aim in this paper is to perform a new step in the analysis of the WP dynamics for hydrogen atom and for ions with one electron by considering spin motion. Until now this effect was not considered for isolated atoms since it requires very long time scales to manifest itself due to the weakness of the spin–orbit coupling. In order to decrease as much as possible this time scale we will consider WP within ions with very large Z. We intended to make a calculation which include all possible effects for these elements and therefore we have considered WP which evolve under the relativistic Dirac Hamiltonian i.e. which are four component spinors.

‖ E-mail: rozmej@tytan.umcs.lublin.pl, mturek@curie.umcs.lublin.pl and arvieu@in2p3.fr

Spin effects and relativistic effects have been studied many times but mostly for atoms submitted to intense laser fields. A recent review has been given in [12]. Some of the most relevant research works are found in [13–16]. It is generally agreed in them that spin and relativistic effects are small but that their magnitude increase with the intensity of the field. For fields of the order of 10^{16} to 10^{17} W/cm^2 they should be taken into account. In a most recent paper [16] the interest has been focussed on the spin–orbit coupling, essentially for Al^{+12} and Ga^{+12} ions. The dynamics of the spin degree of freedom was analyzed there during the time of interaction of the laser with the ion. The authors did not use the Dirac equation but the Schrödinger equation corrected up to order $1/c^3$ and therefore the spin–orbit potential could be clearly identified by its mere suppression. The most significant signature occur in the radiation spectrum. However little polarization was produced for the ions which were considered.

Spin dynamics was previously studied by us in harmonic oscillator potentials in non-relativistic dynamics. In ref. [9–11] we have found a new effect that we have called the *spin–orbit pendulum* for a spin–orbit potential with a constant radial part. This phenomenon is simply the periodic collapse and revival of the average spin and an exchange of angular momentum between spin and the orbital angular momentum. The analysis is quite parallel to that of the Jaynes-Cummings model [17]. In order to extend this situation to a relativistic dynamics it was quite natural to study the Dirac oscillator (DO). There, the strong entanglement that gives rise to spin oscillation is still present [18]. Because of nonlinearities of the relativistic energies the dynamics is not periodic. We have also studied relativistic effects like zitterbewegung. Our studies have been also extended to WP motion corresponding to linear trajectories in non-relativistic approach (HO+LS Hamiltonian) [19] as well as in the relativistic Dirac oscillator [20].

Our previous studies stimulated the present work for hydrogen or for heavy ions. It is expected that many features of the DO should take place in this much more realistic situation.

Our paper is organized as follows. In order to make it self-contained we in Sec. 2 present basic formula for solutions of Dirac equation with Coulomb potential. In Sec. 3 we show the construction of the circular WP and in Sec. 4 we discuss its time evolution, focusing on the autocorrelation function, spin expectation values and spatial motion. Particular attention is paid to relativistic effects and different time scales. The concluding remarks are contained in Sec. 5.

2. Dirac equation with central potential

Solution of Dirac equation for a central field, in particular for Coulomb potential is one of standard, textbook problems in quantum mechanics [21, 22]. Therefore we will recall here only few formula that will be relevant for our further considerations.

Dirac equation for a spherical potential $V(r)$ is

$$H_D\Psi(\boldsymbol{r}) = (c\hat{\boldsymbol{\alpha}}\cdot\boldsymbol{p} + \hat{\beta}mc^2 + V(r))\Psi(\boldsymbol{r}) = E\Psi(\boldsymbol{r})\ . \tag{1}$$

Its eigenfunctions can be found in a representation that diagonalizes simultaneously with H_D three other operators, $\boldsymbol{j}^2, j_z$ and $K = \hbar + \boldsymbol{L}\cdot\boldsymbol{\sigma}$. Then we may write for $\Psi(\boldsymbol{r})$ (using phase convention as in [22])

$$\Psi = \Psi^m_\kappa = \mathrm{i}\begin{pmatrix} g(r)\chi^m_\kappa \\ \mathrm{i}f(r)\chi^m_{-\kappa}\end{pmatrix} = \mathrm{i}\begin{pmatrix} g(r)\Omega_{ljm} \\ \mathrm{i}f(r)\Omega_{l'jm}\end{pmatrix} \tag{2}$$

with

$$l' = 2j - l = \begin{cases} 2(l+\frac{1}{2}) - l = l+1 & \text{for} \quad j = l+\frac{1}{2} = j_+ \\ 2(l-\frac{1}{2}) - l = l-1 & \text{for} \quad j = l-\frac{1}{2} = j_- \end{cases} . \tag{3}$$

The explicit forms of the spherical spinors Ω_{ljm} are:

$$\Omega_{l,j=l+\frac{1}{2},m} = \Omega_{l,j_+,m} = \begin{pmatrix} \sqrt{\frac{j+m}{2j}}\,Y_{l,m-\frac{1}{2}} \\ \sqrt{\frac{j-m}{2j}}\,Y_{l,m+\frac{1}{2}}\end{pmatrix} \tag{4a}$$

and

$$\Omega_{l,j=l-\frac{1}{2},m} = \Omega_{l,j_-,m} = \begin{pmatrix} -\sqrt{\frac{j-m+1}{2j+2}}\,Y_{l,m-\frac{1}{2}} \\ \sqrt{\frac{j+m+1}{2j+2}}\,Y_{l,m+\frac{1}{2}}\end{pmatrix} . \tag{4b}$$

Radial wave functions are given in terms of confluent hypergeometric functions $F(a,c,x)$

$$F(a,c,x) = 1 + \frac{a}{c}x + \frac{a(a+1)}{c(c+1)}\frac{x^2}{2!} + \dots \quad . \tag{5}$$

Explicit formula are [21]:

$$\begin{aligned} f(r) = & -\frac{\sqrt{2}\,\lambda^{5/2}}{\Gamma(2\gamma+1)}\left[\frac{\Gamma(2\gamma+n'+1)(1-E)}{n'!\,\xi(\xi-\lambda/\kappa)}\right]^{\frac{1}{2}}(2\lambda r)^{\gamma-1}\,\mathrm{e}^{-\lambda r} \\ & \times\left[n'F(-n'+1,2\gamma+1,2\lambda r) - (\kappa-\xi/\lambda)F(-n',2\gamma+1,2\lambda r)\right] \end{aligned} \tag{6a}$$

and

$$\begin{aligned} g(r) = & \frac{\sqrt{2}\,\lambda^{5/2}}{\Gamma(2\gamma+1)}\left[\frac{\Gamma(2\gamma+n'+1)(1+E)}{n'!\,\xi(\xi-\lambda/\kappa)}\right]^{\frac{1}{2}}(2\lambda r)^{\gamma-1}\,\mathrm{e}^{-\lambda r} \\ & \times\left[-n'F(-n'+1,2\gamma+1,2\lambda r) - (\kappa-\xi/\lambda)F(-n',2\gamma+1,2\lambda r)\right] , \end{aligned} \tag{6b}$$

where $\xi = Z\alpha$, $\gamma = \sqrt{\kappa^2-\xi^2}$, $\kappa^2 = (j+1/2)^2$, $E = [1+(\frac{\xi}{n'+\gamma})^2]^{-1/2}$ and $\lambda = \sqrt{1-E^2}$, $\alpha = e^2/\hbar c = 1/137.036$ being the *fine structure constant*. The nonnegative integer number n' is related to n and $|\kappa|$ by $n = n' + |\kappa|$. In the following calculations we use atomic units $m_e = \hbar = c = 1$.

3. Construction of wavepacket

In our first paper on relativistic WP in Dirac oscillator (DO) [18] we were considering a circular spinor without small components written as

$$\Psi = \sum_l w_l \begin{pmatrix} a|lll\rangle \\ b|lll\rangle \\ 0 \\ 0\end{pmatrix} = \sum_l w_l\, R_{n=l}(r)|ll\rangle \begin{pmatrix} a \\ b \\ 0 \\ 0\end{pmatrix} . \tag{7}$$

Here a and b are coefficients which determine the initial direction of the spin. There is no loss of generality to choose them real. $R_{n=l}(r)$ denotes radial wave function of the harmonic oscillator. The large component for the partial wave l is written as

$$|ll\rangle \begin{pmatrix} a \\ b \end{pmatrix} = a\Omega_{l,j_+,j_+} + b\left(\frac{\Omega_{l,j_+,j_-} + \sqrt{2l}\,\Omega_{l,j_-,j_-}}{\sqrt{2l+1}}\right) . \tag{8}$$

Weights w_l of the superposition (7) were chosen in a way providing Ψ to be the HO coherent state. For DO the bispinors without small components were constructed as a superposition of spinors with positive and negative energies that provide a cancellation of the small components.

For the Dirac equation with Coulomb potential we are not able to get rid of small components completely, as we want to build the WP only from bound states. We can, however, construct small components in a way similar to the big ones providing their circular motion. For this purpose we write the angular parts of the large components as in eq. (8), then we complete each of the spinors $\Omega_{l,j_+,j_+}, \Omega_{l,j_+,j_-}$ and Ω_{l,j_-,j_-} by their corresponding small components associating each with its radial part different for the states with j_+ and j_- as in eq. (2). Thus there are four radial parts respectively called $g_{j_+}, f_{j_+}, g_{j_-}$ and f_{j_-} for a given l. In order to produce circular waves for hydrogenoid atoms the connection between n and l is $l = n - 1$.

A partial wave at time t can be written with these notations using E_{j_+} and E_{j_-} the eigenvalues of the Dirac equation:

$$\begin{aligned} |\psi_l(t)\rangle = &\left[a\begin{pmatrix} \mathrm{i}\, g_{j_+}\,\Omega_{l,j_+,j_+} \\ -f_{j_+}\,\Omega_{l+1,j_+,j_+} \end{pmatrix} + \frac{b}{\sqrt{2l+1}}\begin{pmatrix} \mathrm{i}\, g_{j_+}\,\Omega_{l,j_+,j_-} \\ -f_{j_+}\,\Omega_{l+1,j_+,j_-} \end{pmatrix}\right] \mathrm{e}^{-\mathrm{i}E_+ t} \\ &+ b\sqrt{\frac{2l}{2l+1}}\begin{pmatrix} \mathrm{i}\, g_{j_-}\,\Omega_{l,j_-,j_-} \\ -f_{j_+}\,\Omega_{l-1,j_-,j_-} \end{pmatrix} \mathrm{e}^{-\mathrm{i}E_- t} . \end{aligned} \tag{9}$$

After expansion of the Ω as in (4*a*,4*b*) the *circular* wavepacket at time t can be written as

$$\Psi(t) = \begin{pmatrix} |c_1(t)\rangle \\ |c_2(t)\rangle \\ |c_3(t)\rangle \\ |c_4(t)\rangle \end{pmatrix} . \tag{10}$$

For Coulomb potential weights w_n (that can be made real) are chosen in a standard way [23, 3, 7], i.e. as a Gaussian distribution with respect to the mean value N:

$$|w_n|^2 = (2\pi\sigma_G^2)^{-\frac{1}{2}}\,\mathrm{e}^{-(n-N)^2/2\sigma_G^2} . \tag{11}$$

Explicit form of the wavepacket (10) is obtained in the following form:

$$\begin{aligned} |c_1(t)\rangle = \mathrm{i}\sum_l w_l \Bigg\{ & g_{j_+}\left[a|l,l\rangle + b\frac{\sqrt{2l}}{2l+1}|l,l-1\rangle\right]\mathrm{e}^{-\mathrm{i}E_{j_+}t} \\ & - b g_{j_-}\frac{\sqrt{2l}}{2l+1}|l,l-1\rangle \mathrm{e}^{-\mathrm{i}E_{j_-}t}\Bigg\} \end{aligned} \tag{12a}$$

$$|c_2(t)\rangle = \mathrm{i}\sum_l w_l\, b|l,l\rangle \left\{ g_{j_+}\frac{1}{2l+1}\mathrm{e}^{-\mathrm{i}E_{j_+}t} + g_{j_-}\frac{2l}{2l+1}\mathrm{e}^{-\mathrm{i}E_{j_-}t}\right\} \tag{12b}$$

$$\begin{aligned}|c_3(t)\rangle = \sum_l w_l \Bigg\{ f_{j_+}\left[a\frac{1}{\sqrt{2l+3}}|l+1,l\rangle + b\sqrt{\frac{2}{(2l+1)(2l+3)}}|l+1,l-1\rangle\right]\mathrm{e}^{-\mathrm{i}E_{j_+}t} \\ -bf_{j_-}\sqrt{\frac{2l}{2l+1}}|l-1,l-1\rangle\mathrm{e}^{-\mathrm{i}E_{j_-}t}\Bigg\}\end{aligned} \tag{12c}$$

$$|c_4(t)\rangle = -\sum_l w_l\, f_{j_+}\left\{a\sqrt{\frac{2l+2}{2l+3}}|l+1,l+1\rangle + b\sqrt{\frac{1}{2l+3}}|l+1,l\rangle\right\}\mathrm{e}^{-\mathrm{i}E_{j_+}t}\,. \tag{12d}$$

For $t = 0$ spin and orbital angular momentum are only approximately decoupled, they were exactly decoupled in (7).

In numerical calculations we use the full bispinor (12*a*-12*d*). However, particularly for $N > 10$, the contributions arising from the small components ($|c_3\rangle$ and $|c_4\rangle$) are almost negligible, because the radial $f(r)$ functions are always few orders of magnitude smaller than the corresponding $g(r)$ functions. This is due to the fact that their prefactors differ mainly by the factor $\sqrt{1-E}$ (few orders of magnitude smaller than 1) for $f(r)$ and $\sqrt{1+E}$ (close to $\sqrt{2}$) for $g(r)$.

Using eqs. (12*c*-12*d*) one can calculate the contributions from small components of our circular WP exactly. One obtains

$$(\Psi^\dagger\Psi)_{small} = \langle c_3(t)|c_3(t)\rangle + \langle c_4(t)|c_4(t)\rangle \tag{13}$$

where

$$\langle c_3(t)|c_3(t)\rangle = \sum_l w_l^2\left\{\left[a^2\frac{1}{2l+3} + b^2\frac{2}{(2l+1)(2l+3)}\right]F_{j_+} + b^2\frac{2l}{2l+1}F_{j_-}\right\}\,, \tag{14a}$$

$$\langle c_4(t)|c_4(t)\rangle = \sum_l w_l^2\left\{a^2\frac{2l+2}{2l+3} + b^2\frac{1}{2l+3}\right\}F_{j_+}\,. \tag{14b}$$

In fact, $(\Psi^\dagger\Psi)_{small}$ $\langle c_3|c_3\rangle$, and $\langle c_4|c_4\rangle$ are constant contributions for our WP. Terms F_{j_-} and F_{j_+} are radial integrals defined in next section. Fig. 1 displays the magnitude of $(\Psi^\dagger\Psi)_{small}$ as function of Z and N for $Z \in [1, 92]$ and $N \in [2, 60]$. Only for very large Z and very small N this contribution exceeds 1%.

4. Wavepacket evolution

4.1. Time scales

We can define several characteristic times on the basis of the previous works about recurrent wave packets [1–7]. Writing the energy in function of a single quantum number n we define for $n = N$ a hierarchy of times

$$\frac{1}{k!}\left(\frac{\mathrm{d}^k E}{\mathrm{d}\, n^k}\right)_{n=N} = \frac{2\pi\hbar}{T(k)} \qquad k = 1, 2, 3, \ldots \tag{15}$$

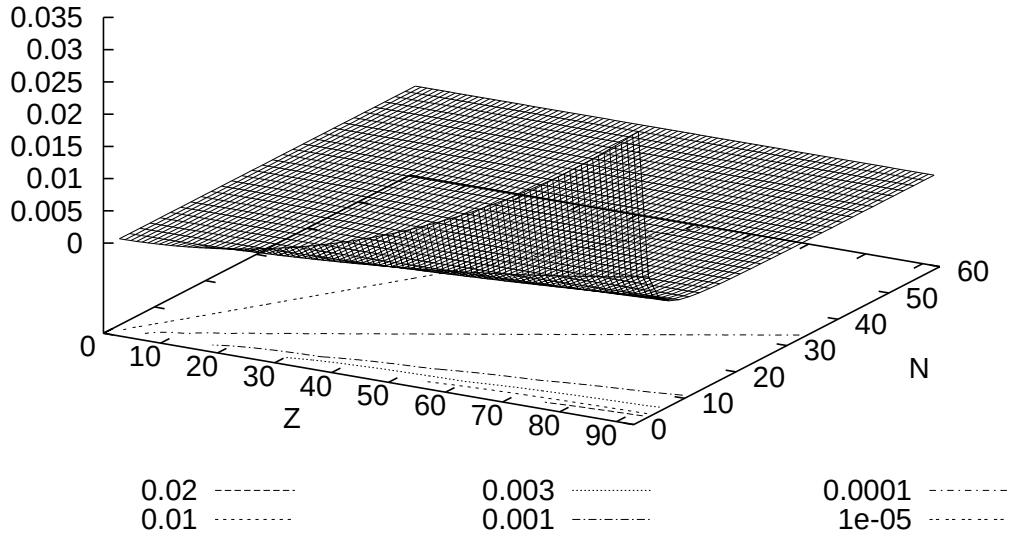

Figure 1. The magnitude of the small components contribution (13) as function of Z and N.

For $k = 1$ we obtain the classical Kepler time, for $k = 2$ the revival time, for $k = 3$ the superrevival time etc...For hydrogenoid atoms those terms increase as N^{k+2}. These times can be compared to a characteristic spin orbit time $T_{ls} = 2\pi/\omega_{ls}$ with ω_{ls} defined by

$$\hbar\omega_{ls} = E_{j_+=N-1/2} - E_{j_-=N-3/2} \; . \tag{16}$$

To first order we obtain

$$\omega_{ls} \approx \frac{(\alpha Z)^2}{N^5} \; . \tag{17}$$

Therefore the spin–orbit frequency follows a variation parallel to the superrevival time with $k = 3$. Those times are plotted on Fig. 2 for $N \geq 2$ and for a large range of atoms (ions) including uranium. For hydrogen T_{ls} is orders of magnitude larger than all the other characteristic times $T(1) - T(5)$. If we want to observe spin–orbit effects in the picosecond regime we can concentrate on $N = 20$ for $Z = 92$. With such a choice $T_{ls} \approx 1685\, T(1)$. The other times are $T_2 = 13.33\, T(1)$, $T_3 = 200\, T(1)$, $T_4 = 3200\, T(1)$. The choice of T_{ls} as a convenient time is justified by our plot of the autocorrelation function of Fig. 3 which shows an interesting oscillations up to 12 periods T_{ls}.

4.2. Autocorrelation function

The autocorrelation function (often referred as the recurrence probability) contain a lot of information on wavepacket evolution. It is a convenient measure of the degree of

recurrences and can be defined as:

$$A(t) = \langle \Psi(0)|\Psi(t)\rangle = \sum_{i=1}^{4} \langle c_i(0)|c_i(t)\rangle \ . \tag{18}$$

Using equations (12*a*-12*d*) one obtains

$$\langle c_1(0)|c_1(t)\rangle = \sum_l w_l^2 \left\{ \left(a^2 + b^2 \frac{2l}{(2l+1)^2} \right) G_{j_+} \mathrm{e}^{-\mathrm{i}E_{j_+}t} \right. \tag{19a}$$
$$\left. + b^2 \frac{2l}{(2l+1)^2} \left[G_{j_-} \mathrm{e}^{-\mathrm{i}E_{j_-}t} - G_{j_\pm} (\mathrm{e}^{-\mathrm{i}E_{j_+}t} + \mathrm{e}^{-\mathrm{i}E_{j_-}t}) \right] \right\} \ ,$$

$$\langle c_2(0)|c_2(t)\rangle = \sum_l w_l^2 \, b^2 \left\{ \frac{1}{(2l+1)^2} G_{j_+} \mathrm{e}^{-\mathrm{i}E_{j_+}t} + \frac{(2l)^2}{(2l+1)^2} G_{j_-} \mathrm{e}^{-\mathrm{i}E_{j_-}t} \right. \tag{19b}$$
$$\left. + \frac{2l}{(2l+1)^2} G_{j_\pm} (\mathrm{e}^{-\mathrm{i}E_{j_+}t} + \mathrm{e}^{-\mathrm{i}E_{j_-}t}) \right\} \ ,$$

$$\langle c_3(0)|c_3(t)\rangle = \sum_l w_l^2 \left\{ \left[a^2 \frac{1}{2l+3} + b^2 \frac{2}{(2l+1)(2l+3)} \right] F_{j_+} \mathrm{e}^{-\mathrm{i}E_{j_+}t} \right. \tag{19c}$$
$$\left. + b^2 \frac{2l}{2l+1} F_{j_-} \mathrm{e}^{-\mathrm{i}E_{j_-}t} \right\} \ ,$$

and

$$\langle c_4(0)|c_4(t)\rangle = \sum_l w_l^2 \left\{ a^2 \frac{2l+2}{2l+3} + b^2 \frac{1}{2l+3} \right\} F_{j_+} \mathrm{e}^{-\mathrm{i}E_{j_+}t} \ . \tag{19d}$$

Terms $G_{j_+}, G_{j_-}, F_{j_+}, F_{j_-}$ and $G_{j_\pm}$ are radial integrals (for instance $G_{j_+} = \int_0^\infty r^2 \, g_{j_+}^2 dr$ and $G_{j_\pm} = \int_0^\infty r^2 \, g_{j_+} g_{j_-} dr$ and so on) that can be easily expressed in terms of Γ functions.

In the presentation of our results below we focus (as in our previous papers) on the most interesting case, i.e. $a = b = 1/\sqrt{2}$. This means that initial direction of the spin is along the Ox axis, in the orbit's plane. In Fig. 3 we present the square of the autocorrelation function $|A(t)|^2$ as function of time for long term evolution (T_{ls} units) of the WP with $N = 20$. Heavy ion system with $Z = 92$ is considered with the full relativistic approach. Very regular revival structure connected with integer values of time in T_{ls} units is immediately recognized. This regularity is somewhat distorted by a strong influence of T_4 periodicity (see right bottom picture of Fig. 2) but becomes even more evident for larger N. Both the main part and the insert of Fig. 3 show very complicated shorter scale behaviour of the autocorrelation function related to the three shorter time scales: T_{cl}, T_{rev}, T_{sr}, known already from the non-relativistic studies [6]. The case with $N = 40$ shown in Fig. 4 suggests that for times $t \in [0, 1.5]\, T_{ls}$ and $t \in [6, 10]\, T_{ls}$ the T_{ls} time scale is essential for the evolution of the WP. It shows also that there exist a deep connection between the time behaviour of the autocorrelation function and the average values of the spin operators as discussed in the next subsection.

4.3. Expectation values of spin operators

Expectation values of spin operators are derived directly from (12*a*-12*d*). One obtains:

$$\langle\sigma_x\rangle_t = \sum_l w_l^2 \left\{ \frac{2ab}{2l+1}(G_{j_+} + 2lG_{j_\pm} \cos\omega_l t) - \frac{2ab}{2l+3}F_{j_+} \right\} + \delta\sigma_x \ , \tag{20a}$$

$$\langle\sigma_y\rangle_t = \sum_l w_l^2 \left\{ 2ab\frac{2l}{2l+1}G_{j_\pm} \sin\omega_l t \right\} + \delta\sigma_y \ , \tag{20b}$$

$$\begin{aligned}\langle\sigma_z\rangle_t = \sum_l w_l^2 \Bigg\{ & a^2 G_{j_+} + b^2\frac{2l-1}{(2l+1)^2}(G_{j_+} - 2lG_{j_-}) - b^2\frac{8l}{(2l+1)^2}G_{j_\pm}\cos\omega_l t \\ & + b^2\frac{2l}{2l+1}F_{j_-} - \left(a^2\frac{2l+1}{2l+3} + b^2\frac{2l-1}{(2l+1)(2l+3)}\right)F_{j_-} \Bigg\} \ ,\end{aligned} \tag{20c}$$

where $\omega_l = (E_{j_+} - E_{j_-})/\hbar$. Terms denoted by $\delta\sigma_x$ and $\delta\sigma_y$, which are only small contributions, stem from coupling between states with l or j different by 2 units. Their explicit expressions are:

$$\delta\sigma_x = \sum_l K_l \cos\tilde{\omega}_l t \ , \tag{21a}$$

$$\delta\sigma_y = \sum_l K_l \sin\tilde{\omega}_l t \ , \tag{21b}$$

where

$$\hbar\tilde{\omega}_l = E_{j_+} - E_{(j+2)_-} \ , \tag{22a}$$

$$F' = \int_0^\infty r^2 \, f_{j+} f_{(j+2)_-} dr \ , \tag{22b}$$

and

$$K_l = 2ab\, w_l w_{l+2}\, F' \sqrt{\frac{(2l+2)(2l+4)}{(2l+3)(2l+5)}} \ . \tag{22c}$$

In a non-relativistic limit the terms containing the radial parts f_{j_+} and f_{j_-} cancel and the correction terms $\delta\sigma_x$ and $\delta\sigma_y$ tend to zero, the same for F_{j_+} and F_{j_-}. For the harmonic oscillator with a constant spin–orbit potential the radial integrals verify

$$G_{j_+} = G_{j_-} = 1 \ . \tag{23}$$

The dynamics of the spin motion in such a case has been discussed by us in [9] and [10]. Using the dispersion law appropriate to a constant spin–orbit potential

$$\omega_l = (2l+1)\omega_{ls} \tag{24}$$

we have obtained there the periodic oscillations between spin and orbital angular momentum that we have called *spin–orbit pendulum*.

In the present, more general case we see that both $\langle\sigma_x\rangle$ and $\langle\sigma_z\rangle$ contain an additional constant shift with respect to the non-relativistic expressions, coming clearly from the small components. In addition there are time dependent shifts due to the $\delta\sigma_x$

and $\delta\sigma_y$ terms. Numerically these shifts may be safely neglected. Therefore the most interesting dependence comes from the use of the eigenvalues of the Dirac hamiltonian in the time behaviour that we will now discuss in more details.

In Figs. 5 and 6 we present the average values of the spin operators and the length of the spin vector as functions of time for cases $N = 20$ and $N = 40$ ($Z = 92$). The latter case the most distinctly reminds both non-relativistic *spin–orbit pendulum* for the HO+LS Hamiltonian [9,10] and the relativistic one for the DO [18]. We clearly recognize time ranges for the spin collapse ($0 \leq t \leq 2.5$), strong spin entanglement ($2.5 \leq t \leq 4.5$) and spin revivals ($6 \leq t \leq 10$, all times in T_{ls} units). For the case $N = 20$, shown in Fig. 5, we see a similar behaviour of the spin averages, distorted, however, much more due to stronger interferences with T_4 characteristic time. In cases discussed above the ratio T_4/T_{ls} is approximately equal to 1.9 for $N = 20$ and 3.7 for $N = 40$.

4.4. Spatial motion of circular WP

Let us now discuss the motion of WP in space. A complex structure of the autocorrelation function and the existence of several time scales suggest that qualitatively similar spatial evolution can occur in different time scales. Below we focus our presentation of the probability density motion in two particular time scales: the shortest one, corresponding to the Kepler period of classical electron motion on the circular orbit with $n = N$, and the spin–orbit motion time scale. The admixture of the components $|l, l-1\rangle$ in $|c_1(t)\rangle$ $(12a)$ [as shown earlier the small components give negligible contributions to $\Psi^\dagger\Psi$] causes deviations of the WP motion from the equatorial plane, known already from our previous non-relativistic studies [11,24]. The magnitude of these deviations decreases, however, when N increases and for $N \geq 10 - 12$ the maximum of the probability density moves very close to the equatorial plane, i.e. the plane of the classical orbit. Therefore we limit our presentation of $[\Psi^\dagger\Psi](t)$ to this plane only. For the short time scale, $t \in [0, 9/4]\, T_{cl}$, it is shown in Fig. 7. The sequence of pictures exhibits the behaviour known from non-relativistic studies on WP in hydrogen atom [23, 3, 7, 1, 2, 4, 5], namely circular motion with spreading along the orbit and forming interference patterns that lead to fractional revivals. n Fig. 7 we display the full probability density $\Psi^\dagger\Psi$, not the spin up and spin down components separately, because for such short time scale no difference in their motion is visible.

In order to see this difference one needs to observe WP in time scale comparable to T_{ls}. In Fig. 8 we present the sequence of shapes of the same WP ($N = 20, Z = 92$) for times $t = 0, 1/2, 1, 3/2$ and 2 (in T_{ls} units). In these cases the presentation is divided into the two parts: in the left column spin up components of $\Psi^\dagger\Psi$ are displayed, whereas in the right column the spin down components are shown. At the presented time instants, that are multiples of $T_{ls}/2$ both sub-packets are quite well revived (localized) and move on a circle with different velocities.

Fig. 9 shows (in the same convention) the shapes of WP's components with spin up (left) and spin down (right) for time $t = 10.063545\, T_{ls}$ ($N = 20, Z = 92$). As seen

from Fig. 3 this time corresponds to the highest value of the autocorrelation function ($|A(t)|^2 \approx 0.8$) in the presented range of times. One sees from this figure that the degree of the recurrences (of both sub-packets separately) is indeed very high in this case.

5. Conclusions

We have discussed the full 3+1–dimensional evolution of the relativistic wave packets in Coulomb potential. The main relativistic effect is the appearance of the new time scale due to the spin–orbit coupling. In general this effect has the same origin as *spin–orbit pendulum*, introduced by us both in non-relativistic [9–11] and relativistic [18] studies, where harmonic oscillator potential with a strong spin–orbit coupling was considered. In the Coulomb potential (relativistic) case presented here the time scale of the spin–orbit motion is large, therefore there is practically no chance for observing it in such systems like hydrogen or hydrogenoid atoms. However, this time scale decreases rapidly as function $1/Z^2$, when heavy ions with the single electron are considered as systems for experimental studies. At $Z = 82$, and even better $Z = 92$ the T_{ls} time becomes reasonably short and in principle experimental observations of the spin–orbit effects in electron WP's motion may become possible with existing techniques. This conclusion is based on the fact that the single electron heavy ions with $Z = 82, 92$ have been already created and some of their properties have been measured [25]. It is also possible to suitably adjust the two parameters N, Z in order to fit the energies of electron states and time scales of the motion to ranges of action of available lasers that have to be used for creation of wave packets and analysis of their motion.

Comparing the phenomenon of the *spin–orbit pendulum* discussed in our previous studies [9–11, 18] with the present Coulomb potential case one sees the following differences. During their motion Coulomb wave packets experience several important time scales (only one is present in the HO case) that make the motion much more complex and obscure the spin–orbit motion. Relativistic (nonlinear) dependence of the eigenenergies on quantum numbers destroy exact periodicity of the motion.

Acknowledgment

P.R. and M.T kindly acknowledge financial support (in part) of Polish Committee for Scientific Research (KBN) under the grant 2 P03B 143 14.

References

[1] Parker J and Stroud Jr. CR 1986 *Phys. Rev. Lett.* **56** 716
[2] Averbukh IS and Perelman NF 1989 *Phys. Lett.* **A139** 449; 1989 *Zh. Eksp. Teor. Fiz.* **96** 818: (1989 *Sov. Phys. JETP* **69** 464); 1991 *Usp. Fiz. Nauk* **161** 41, (1991 *Sov. Phys. Usp.* **34** 572).
[3] Nauenberg N 1990 *J. Phys. B: At. Mol. Opt. Phys.* **23** L385
[4] Dačic-Gaeta Z and Stroud Jr. CR 1990 *Phys. Rev.* **A42** 6803
[5] Peres A 1993 *Phys. Rev.* **47** 5196

[6] Bluhm R and Kostelecky VA 1994 *Phys. Rev. A* **50** R4445; 1995 *Phys. Lett. A* **200** 308; 1995 *Phys. Rev. A* **51** 4767
[7] Bluhm R Kostelecky VA and Porter JA 1996 *Am. J. Phys.* **64** 944
[8] Alber G and Zoller P 1991 *Phys. Reports* **5** 231;
Garraway BM and Suominen KA 1995 *Rep. Prog. Phys.* **58** 365
[9] Arvieu R and Rozmej P 1994 *Phys. Rev.* A **50** 4376
[10] Arvieu R and Rozmej P 1995 *Phys. Rev.* A **51** 104
[11] Rozmej P and Arvieu R 1996 *J. Phys. B: At. Mol. Opt. Phys.* **29** 1339
[12] Protopapas M, Keitel CH, Knight PL 1997 *Rep. Prog. Phys.* **60** 389
[13] Latinne O, Joachain CJ and Dorr M 1994 *Europhys. Lett.* **26** 333
[14] Rathe UW, Keitel CH, Protopapas M and Knight Pl 1997 *J. Phys. B: At. Mol. Opt. Phys.* **30** L531
[15] Szymanowski C, Veniard V, Taieb R, Maquet a and Keitel CH 1997 *Phys. Rev.* **A56** 3846
[16] Hu SX and Keitel CH 1999 *Phys. Rev. Lett.* **83** 4709
[17] Jaynes ET and Cummings FW 1963 *Proc. IEEE* **51** 89
[18] Rozmej P and Arvieu R 1999 *J. Phys. A: Math. Gen.* **32** 5367
[19] Arvieu R, Rozmej P and Berej W 1997 *J. Phys. A: Math. Gen.* **30** 5381
[20] Turek M, Rozmej P and Arvieu R 2000 *Acta Phys. Polon.* B, in print
[21] Rose ME 1966? *Relativistic Electron Theory* (New York: John Wiley & Sons)
[22] Greiner W 1990 *Relativistic Quantum Mechanics, Wave Equations* (Berlin: Springer)
[23] Brown LS 1973 *Am. J. Phys.* **41** (1973) 525
[24] Rozmej P and Arvieu R 1996 *Acta Phys. Polon. B* 581
[25] Stöhlker, Ionescu DC, Rymuza P, et. al. 1998 *Phys. Lett. A* **238** 43;
Stöhlker, Bosch F, Dunford RW, et. al. 1999 *Physica Scripta* **T80B** 379

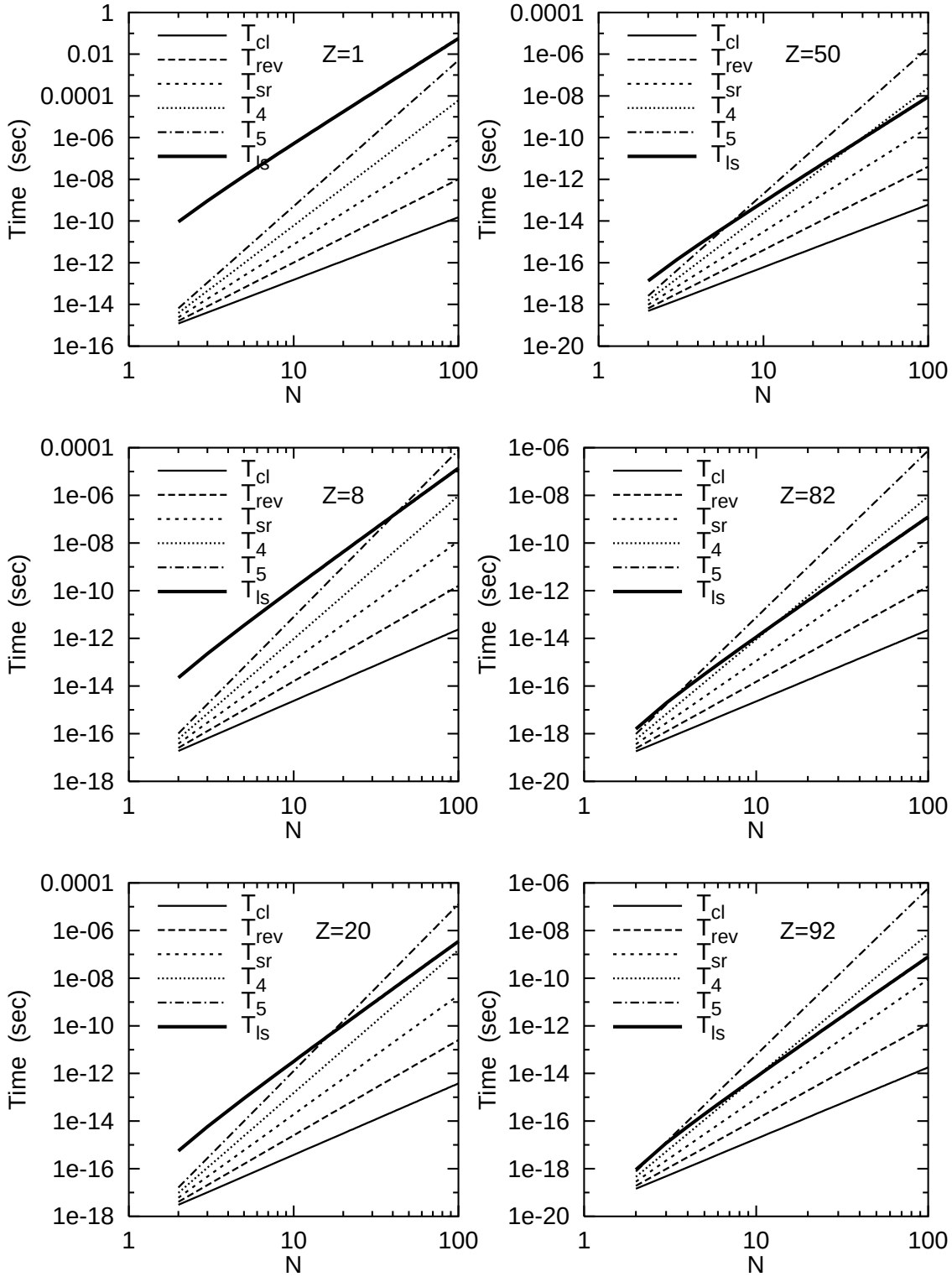

Figure 2. Characteristic times of the WP evolution as functions (in log–log plot) of the mean value of principal quantum number for different values of nuclear charge (from $Z = 1$ to 92). The period of spin–orbit motion is given by the thick solid line.

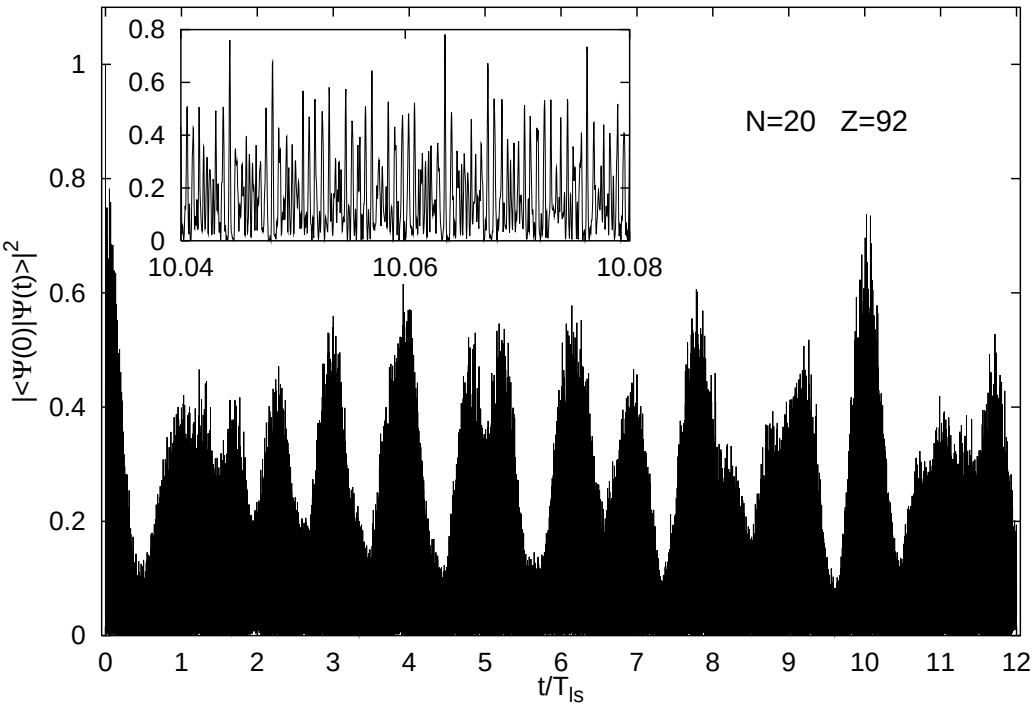

Figure 3. Square of the autocorrelation function for system with $N = 20$, $Z = 92$ for long term evolution. In this case $T_{ls} \approx 1685\, T_{cl}$, where $T_{cl} = 2\pi\, N^3/(Z\alpha)^2$ is a Kepler time for non-relativistic WP with the same N. Short term behaviour around the best revival is presented in the insert.

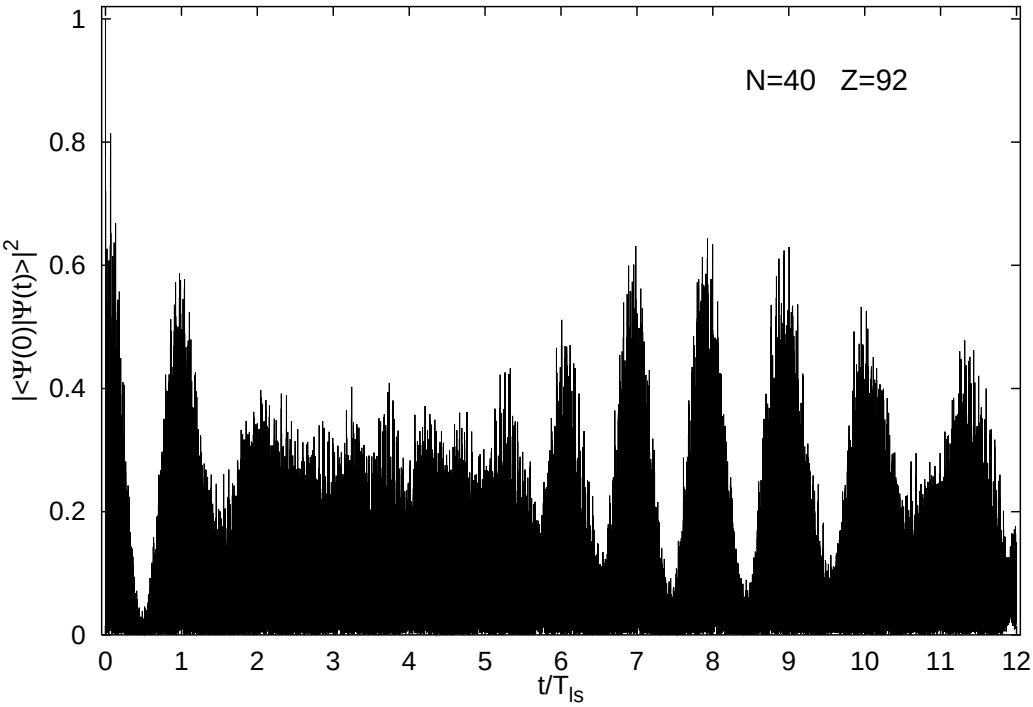

Figure 4. Square of the autocorrelation function for system with $N = 40$, $Z = 92$ for long term evolution. In this case $T_{ls} \approx 6921\, T_{cl}$.

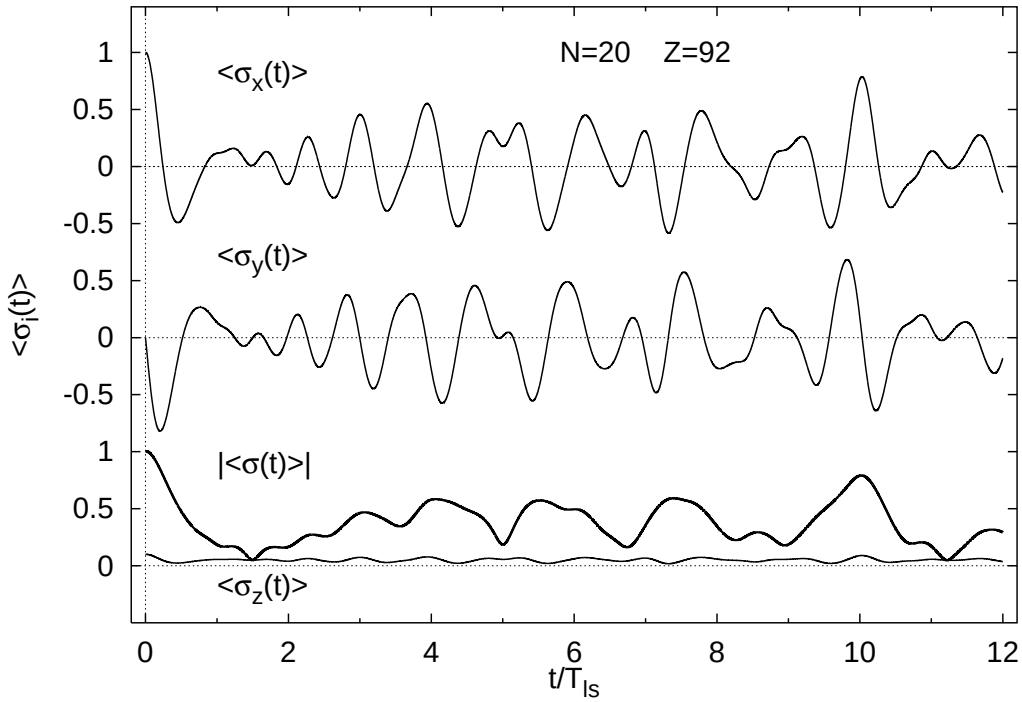

Figure 5. Time evolution of the average values of spin components $\langle\sigma_i\rangle$, $i = x, y, z$ for system with $N = 20$, $Z = 92$.

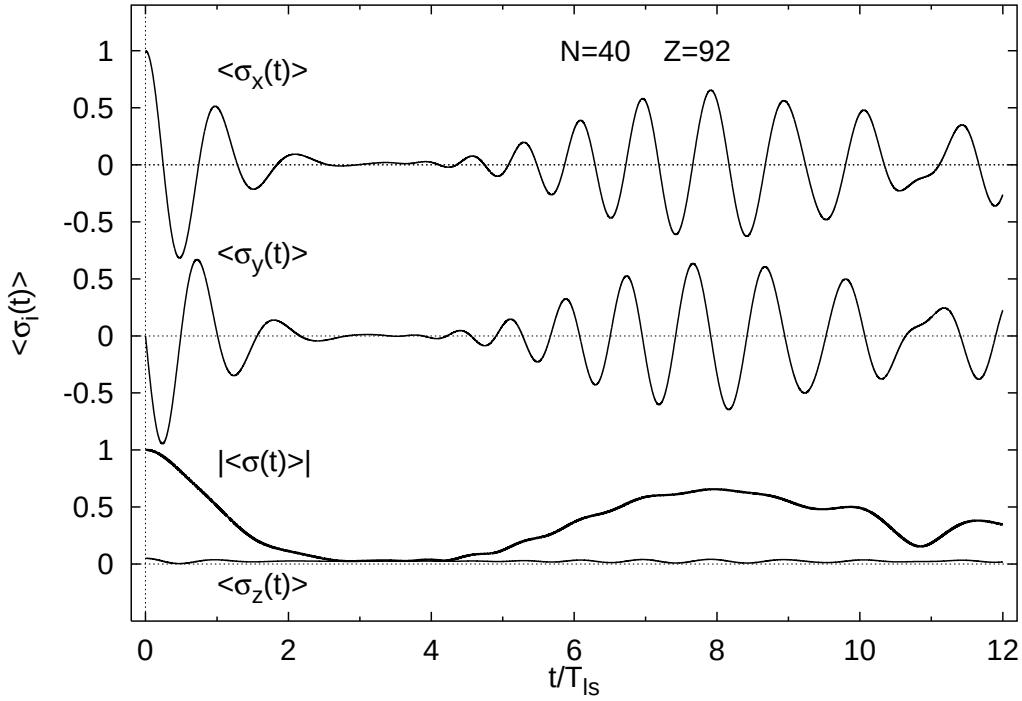

Figure 6. Time evolution of the average values of spin components $\langle\sigma_i\rangle$, $i = x, y, z$ for system with $N = 40$, $Z = 92$.

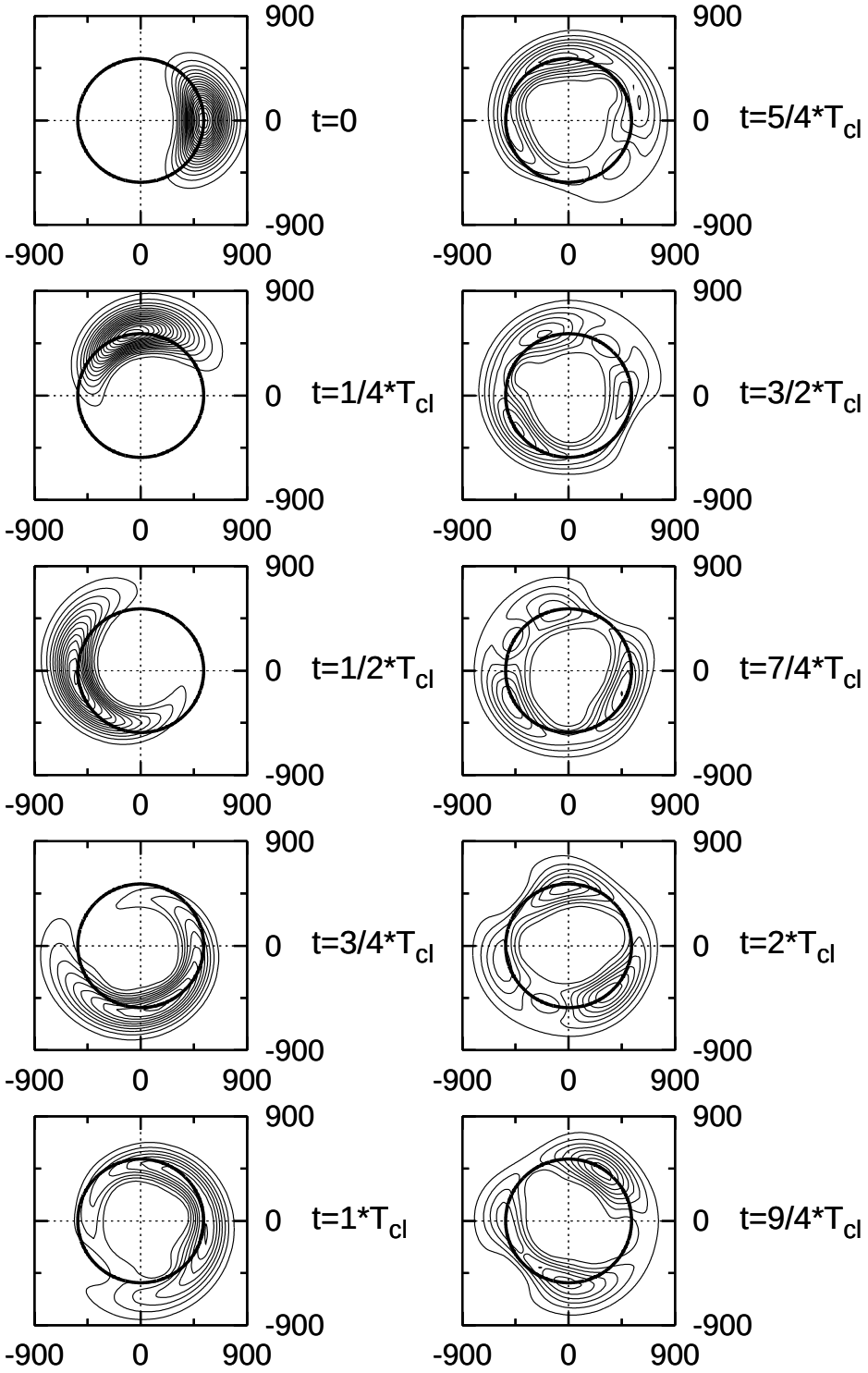

Figure 7. Spatial motion of the WP with $N = 20$, $Z = 92$ in the initial stage of time evolution $t \in [0, 9/4]T_{cl}$. The probability density $\Psi^\dagger\Psi$ is plotted as function of the position on the plane of the electron's classical orbit. The radius of the thick circle corresponds to the initial distance of the WP's peak from the center of the potential. Note that in this figure and all next plots the contour lines correspond to the same values of the probability density.

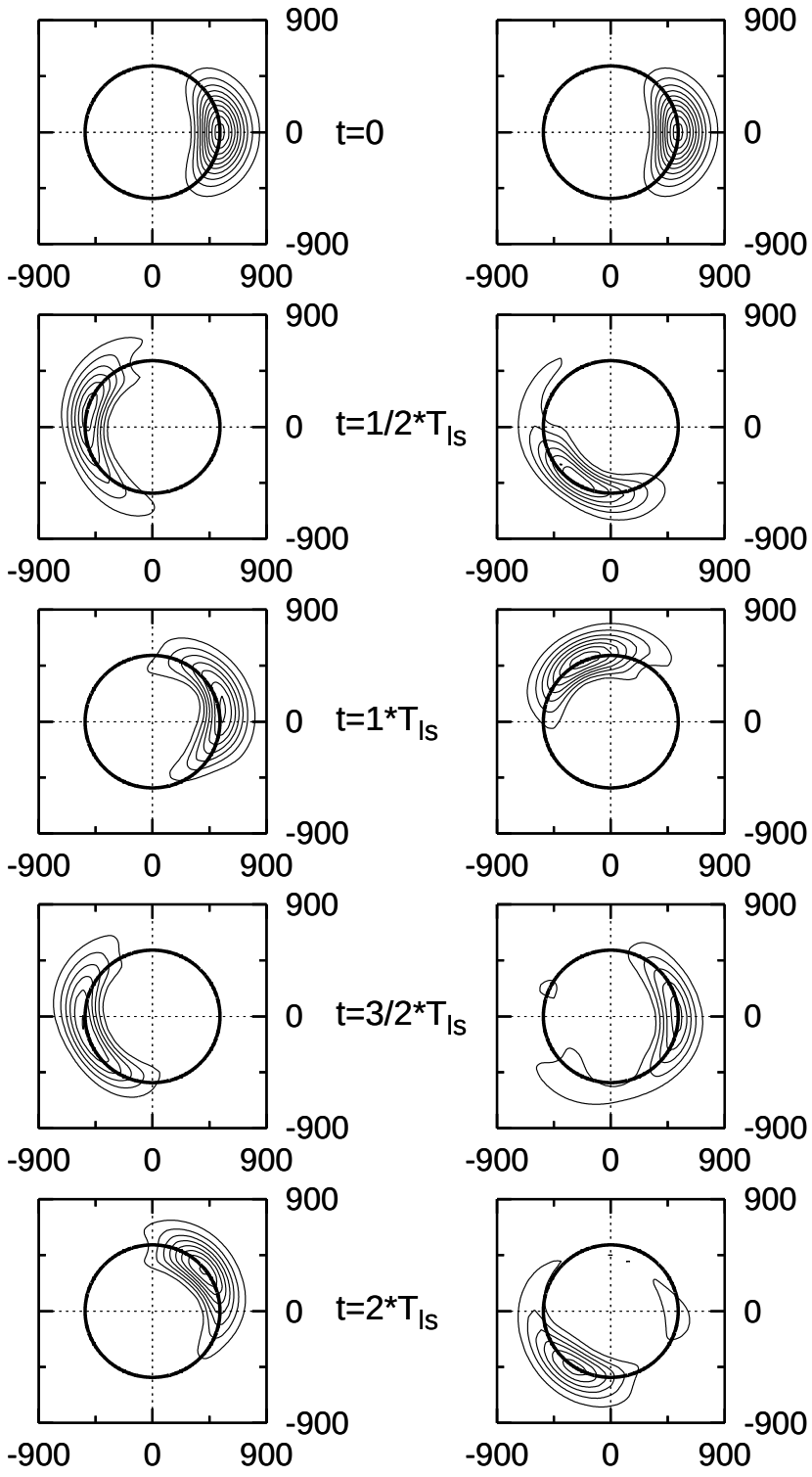

Figure 8. Shapes of the WP ($N = 20, Z = 92$) components with spin up (left column) and spin down (right column) during evolution in time scale measured in T_{ls} units ($t \in [0, 2]T_{ls}$). The different angular velocities of the motion of these sub-packets are clearly visible.

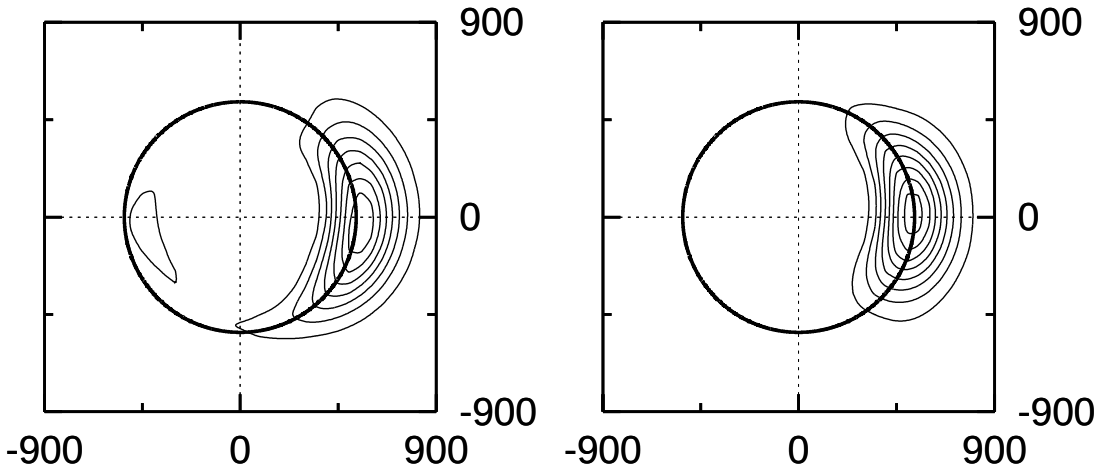

Figure 9. The best revival of the WP for the system with $N = 20$, $Z = 92$ presented on the plane of the classical orbit. The time instant $t = 10.063545\,T_{ls}$ corresponds to the highest value of the autocorrelation function displayed in Fig. 3. For comparison with the spin components at $t = 0$ see the upper row of the Fig. 7